Naval Research Laboratory
Stennis Space Center, MS 39529-5004

AD-A274 535

NRL/MR/7240--93-7072

The Hough Transform Algorithm for Sea Ice Lead Analysis: An Evaluation

DENISE J. GINERIS

Sverdrup Technology
Stennis Space Center, MS 39522-5004

FLORENCE M. FETTERER

Remote Sensing Applications Branch
Remote Sensing Division

November 15, 1993

32pg 94-01106

94 1 10 096

DISCLAIMER NOTICE

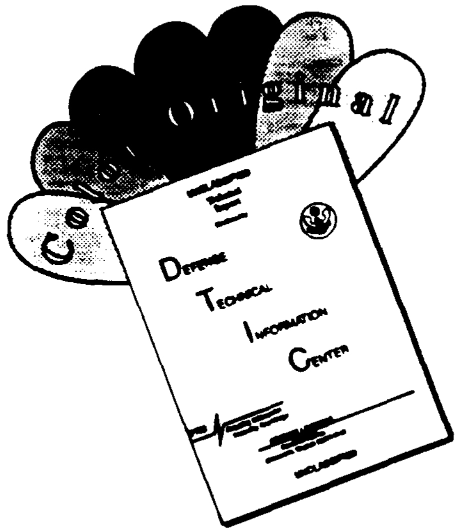

THIS DOCUMENT IS BEST QUALITY AVAILABLE. THE COPY FURNISHED TO DTIC CONTAINED A SIGNIFICANT NUMBER OF COLOR PAGES WHICH DO NOT REPRODUCE LEGIBLY ON BLACK AND WHITE MICROFICHE.

REPORT DOCUMENTATION PAGE

Form Approved
OBM No. 0704-0188

1. Agency Use Only *(Leave blank).*

2. Report Date.
November 15, 1993

3. Report Type and Dates Covered.
Final

4. Title and Subtitle.
The Hough Transform Algorithm for Sea Ice Lead Analysis: An Evaluation

5. Funding Numbers.
Program Element No. 0603207N
Project No. X1596
Task No.
Accession No. DN258116
Work Unit No. 72-5189-04

6. Author(s).
Denise J. Gineris and Florence M. Fetterer*

7. Performing Organization Name(s) and Address(es).
Sverdrup Technology
Stennis Space Center, MS 39522-5004

8. Performing Organization Report Number.
NRL/MR/7240--93-7072

9. Sponsoring/Monitoring Agency Name(s) and Address(es).
Space and Naval Warfare Systems Command
2451 Crystal Drive
Arlington, VA 22202

10. Sponsoring/Monitoring Agency Report Number.
NRL/MR/7240--93-7072

11. Supplementary Notes.
*Naval Research Laboratory
Stennis Space Center, MS 39522-5004

12a. Distribution/Availability Statement.
Approved for public release; distribution is unlimited.

12b. Distribution Code.

13. Abstract *(Maximum 200 words).*

An algorithm for sea ice lead analysis using a Hough transform technique has been developed at the Naval Research Laboratory (NRL) Remote Sensing Applications Branch and is currently in use at NRL and the Navy/National Oceanic and Atmospheric Administration (NOAA) Joint Ice Center (JIC). The algorithm resides on a Sun microcomputer system as part of a larger image processing package (the NRL Satellite Image Processing System or NSIPS) developed at NRL. Currently, the algorithm functions on Advanced Very High Resolution Radiometer (AVHRR) and Operational Line Scan imagery. Algorithm performance was evaluated by comparing results from the Hough transform technique to those obtained through manual analysis for a set of five AVHRR infrared images. The algorithm operated well, but there is still room for improvement. Details of the evaluation and recommendations for improvement are contained in this report.

14. Subject Terms.
remote sensing, SAR, ERS-1, sea ice

15. Number of Pages.
29

16. Price Code.

17. Security Classification	18. Security Classification of Report.	19. Security Classification of This Page.	20. Limitation of Abstract. of Abstract.
Unclassified	Unclassified	Unclassified	SAR

NSN 7540-01-280-5500

Standard Form 298 (Rev. 2-89)
Prescribed by ANSI Std. Z39-18
298-102

Contents

The Hough Transform Algorithm for Sea Ice Lead Analysis: An Evaluation

1.0 Introduction

The analysis of leads in the Arctic ice pack is a crucial part of arctic ice studies. Open leads, as well as those with new ice, play an important role in global heat exchange. In addition, knowledge of lead size and dynamics are important to ship routing in the region. Satellite sensors operating in the visible, infrared, and microwave wavelength bands routinely image the arctic area, providing a copious amount of lead data. Algorithms have been developed to aid in the analysis of these data by providing ice parameters such as ice concentration, ice edge, lead orientation and lead size semi-automatically. One such algorithm for lead analysis is the Hough transform technique developed by Fetterer and Holyer (1989). The purpose of this report is to present the results of an evaluation of this technique as it is applied to infrared imagery collected by the Advanced Very High Resolution Radiometer (AVHRR) on the NOAA polar-orbiting series of satellites.

2.0 Description of the Algorithm

The Hough transform is a technique used in image processing to detect linear features. In general, the transform is applied to image pixels which have already been identified as pixels of interest. Each pixel of interest, or feature pixel, at a given position x,y in an image is mapped into (ρ,θ) parameter space using the normal parameterization of a line:

$$\rho=x\cos(\theta)+y\sin(\theta),$$

where ρ is the distance from the image origin (defined as an image corner) to position x,y and θ is the angle from the horizontal to ρ. Paired with this parameter space is an accumulator array whose size is equal to that of parameter space. For every feature pixel, 180 pairs of ρ and θ are generated; θ is taken from 0 to 180 degrees in one degree steps and an ρ value is calculated for each θ value. The representation of the x,y feature pixel in (ρ,θ) space is thus a sinusoidal curve (see Figure 1). At every position along the sinusoidal curve in parameter space the accumulator array is incremented by one.

Every feature pixel has a sinusoidal curve in (ρ,θ) parameter space associated with it. Every (ρ,θ) position along the curve represents a series of lines which can go through a particular feature pixel at position x,y. If several feature pixels are part of the same linear feature, as in figure 1, their sinusoidal curve representations in (ρ,θ) space will intersect at the (ρ,θ) point which represents the line which goes through all feature pixels. The value of the accumulator array at that particular (ρ,θ) point would be equal to the sum of the sinusoidal curves which intersect at that (ρ,θ) point, or the number of feature pixels on that line. The more sinusoidal curves which intersect, the higher the accumulator array value, and the higher the accumulator array value, the more probable the chance that a linear feature exists in the image. The orientation of the linear feature is given by the value of θ at the accumulator peak location, while the size of the peak is an indication of the size of the feature.

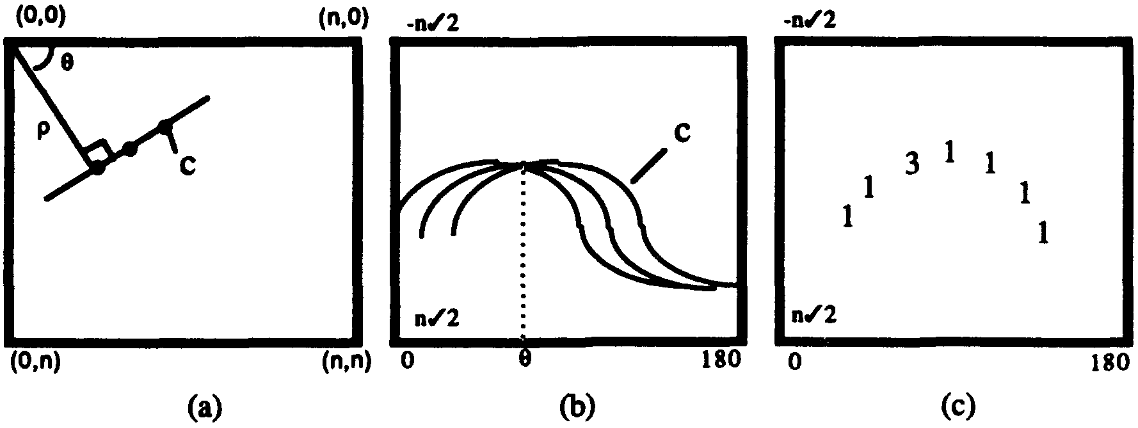

Figure 1. Illustration of the Hough transform technique: (a) a line of feature pixels in the image, (b) representation of the linear feature as a series of sinusoidal curves, point C is associated with curve C, (c) the values along curve C in accumulator space. The point with a value of 3 is the accumulator peak in this case.

As applied to the case of AVHRR imagery of leads, the procedure of the Hough transform technique is as follows. First the selected ice lead image undergoes a Wallis filter to enhance linear features and reduce the effects of uneven image intensity due to thin cloud layers, variations in ice type or other causes of temperature gradients. Cloud contaminated areas are then masked by hand, and a binary threshold is applied to the image to produce a binary product with leads in white and all other features in black. This is possible because leads are bright features in infrared imagery, being much warmer than the surrounding ice. The Hough transform is then performed on this binary product, converting the linear image features represented in the binary product into peaks in accumulator space. Peaks above a certain threshold value are assumed to be lead segments, which are the linear portions of a lead between lead endpoints, junction points, or flexure points. The peaks in accumulator space may be wide due to a variety of reasons such as the width of the image lead feature and curvature of the lead. This smearing is compensated for by the application of a clustering algorithm which replaces a cluster of accumulator peaks with a single peak equal in value to the sum of the peaks in the cluster. This summed value is equated to the lead segment size (area in square kilometers, given 1 km AVHRR pixels) and lead segment orientation is given by the complement of the θ value of the single summed peak (90 degrees minus θ). A noise threshold is applied to remove spurious peaks of non-lead origin. False detections, which occur when isolated pixels are colinear but do not belong to the same lead, are avoided by computing Hough transform for smaller 64x64 pixel subsections of the image, instead of for the whole image. See Fetterer, Pressman, and Crout (1990) for further discussion of the application of the algorithm to AVHRR data.

The transform process provides two outputs to the user. The first is a listing, for each 64x64 pixel block processed, of the total lead segment size as a function of lead segment orientation (Figure 2). It should be noted that the present form of the algorithm does not distinguish between independent lead segments with identical orientations. They are represented in the output file as one lead segment whose size is the sum of all. The second output is an image file which contains a series of rose plots, one for every 64x64 pixel block (Figure 3). Red lines in the rose plots represent lead segments whose areas are less than the outer circle of the rose plot (in this case, $50km^2$), and yellow lines represent those lead segments whose areas are greater than the outer circle. This image file conveys the same information as the lead segment listing, but in a visual format, which is easier to compare to the actual image.

3.0 Description of the Data

For this analysis, a data set was chosen from AVHRR infrared imagery collected in the late winter/early spring of 1990 over Greenland and in the late winter/early spring of 1992 in the Beaufort Sea. Five images were selected which were relatively cloud free and exhibited a variety of lead features. These images are illustrated in Figures 4 through 8 as pairs of the original AVHRR infrared data (channel 4, 10.362-11.299 μm) and their corresponding binary products. The lead features represented by this data set range in orientation from vertical to horizontal, and in length from about 10 km to 500 km. Both straight and curvilinear leads are represented, as are a variety of lead widths, ranging from one kilometer (the pixel resolution) to about 7 kilometers. In addition, a few spurious features were included to test the robustness of the Hough transform technique in the presence of false features. The two most notable of these features are a cluster of first year ice areas in the image from March 29, 1992, and an area of water vapor in the image from March 18, 1990, both of which a human interpreter could easily recognize as non-leads. Collection and processing details for these images are presented in Table 1.

Table 1. Images used in the evaluation.

Date	Time (GMT)	Location	Pixel Resolution (km)
12 January 1990	1545	Lincoln Sea	1.1
18 March 1990	1553	Lincoln Sea	1.1
3 April 1990	1442	Lincoln Sea	1.1
29 March 1992	1336	Beaufort Sea	1.0
7 April 1992	1510	Beaufort Sea	1.0

4.0 Description of the Analysis

The Hough transform was applied to each of these images and the results were obtained in the form of rose plots of total lead segment size versus orientation for each 64x64 pixel block and list files in ASCII format which provide block number, orientation, and total segment size. Figures 2 and 3 provide examples of the list file and rose plot results of the Hough transform. For each block analyzed, four parameters were calculated from the results of both the Hough transform technique and a manual lead analysis, and compared. These parameters were: 1) total lead segment size (area in km^2), 2) total number of lead segments, 3) mean lead segment size, and 4) weighted mean lead segment orientation. Weighted mean orientations (vector averages) were used as they are geophysically more accurate than unweighted mean orientations. Lead length was not included, since the results from the Hough algorithm do not produce that parameter. This comparison of the lead parameters accumulated for each 64x64 pixel block served to provide a general test of the robustness of the Hough transform technique. More detailed comparisons were achieved through the analysis of histograms of lead segment size and orientation for each image as a whole. This image by image histogram comparison of manual and algorithm results provided

Text Editor: /sid1/gineris/leads/03apr90.lss

Input file name = /sid1/gineris/03apr90bin.rc^@

Block Number	Direction	km^2
1	3.0	92.0
1	11.0	25.0
1	17.0	9.0
1	45.0	10.0
1	51.0	50.0
1	113.0	15.0
1	118.0	10.0
1	136.0	21.0
1	141.0	10.0
1	153.0	35.0
1	163.0	50.0
1	168.0	90.0
1	173.0	81.0
1	176.0	85.0
2	3.0	14.0
2	25.0	83.0
2	34.0	9.0
2	39.0	84.0
2	45.0	8.0
2	47.0	28.0
2	125.0	9.0
2	134.0	34.0
2	138.0	115.0
2	142.0	11.0
2	146.0	19.0
2	152.0	36.0
2	163.0	17.0
2	167.0	35.0
2	179.0	8.0
3	3.0	8.0
3	8.0	19.0
3	25.0	33.0
3	37.0	9.0
3	39.0	11.0
3	43.0	18.0
3	134.0	12.0
3	138.0	18.0
3	143.0	8.0
3	151.0	9.0
3	160.0	41.0
3	164.0	116.0
3	179.0	12.0
4	3.0	36.0
4	8.0	12.0
4	9.0	16.0
4	16.0	8.0
4	24.0	160.0
4	32.0	15.0
4	45.0	14.0
4	143.0	8.0
4	154.0	11.0
4	160.0	42.0
4	162.0	26.0
4	173.0	27.0
4	176.0	16.0

Figure 2. Example of a Hough transform list file.

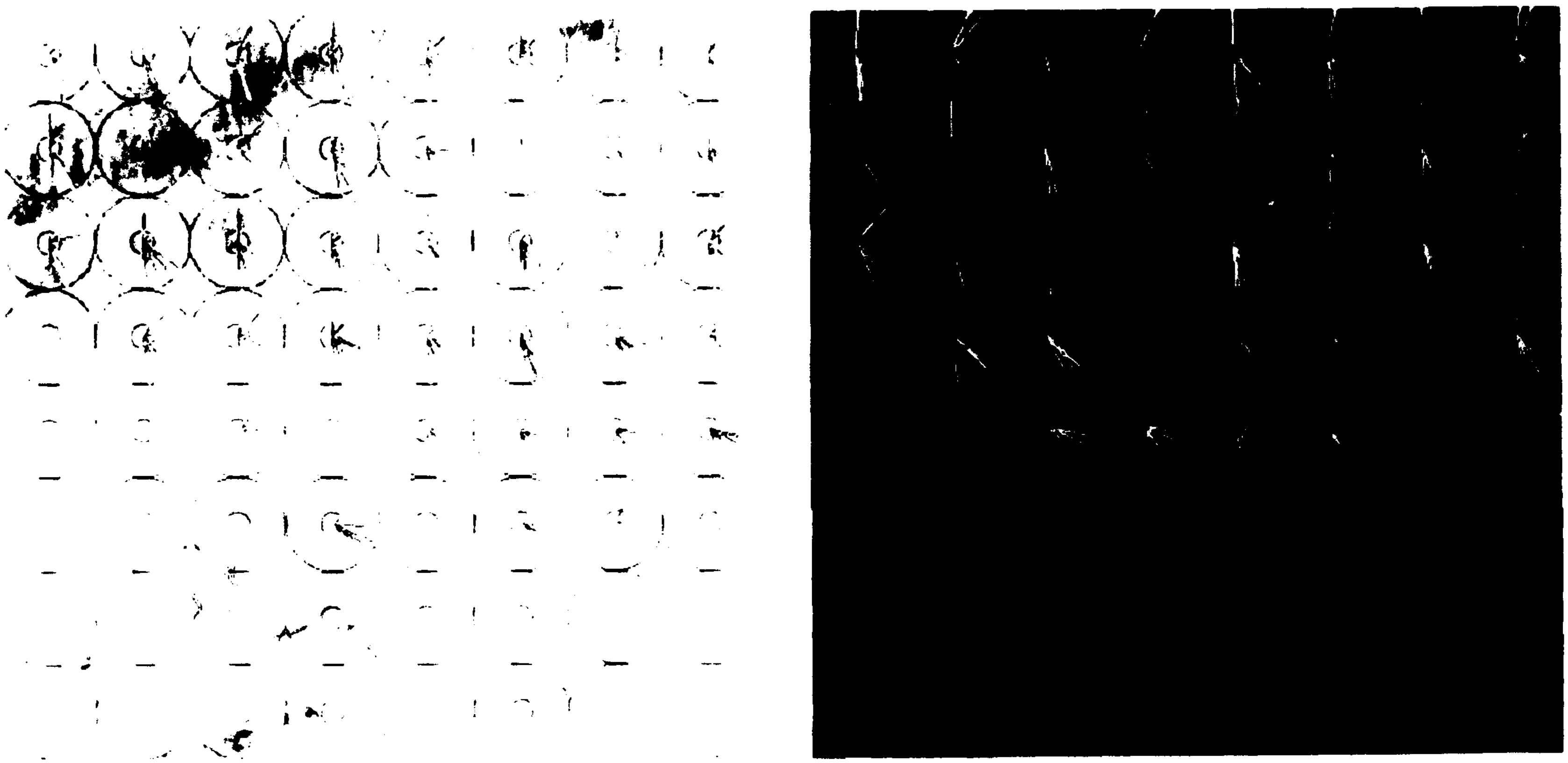

(a) (b)

Figure 3. Example of a Hough transform rose plot: (a) AVHRR image overlain with rose plot, (b) rose plot alone.

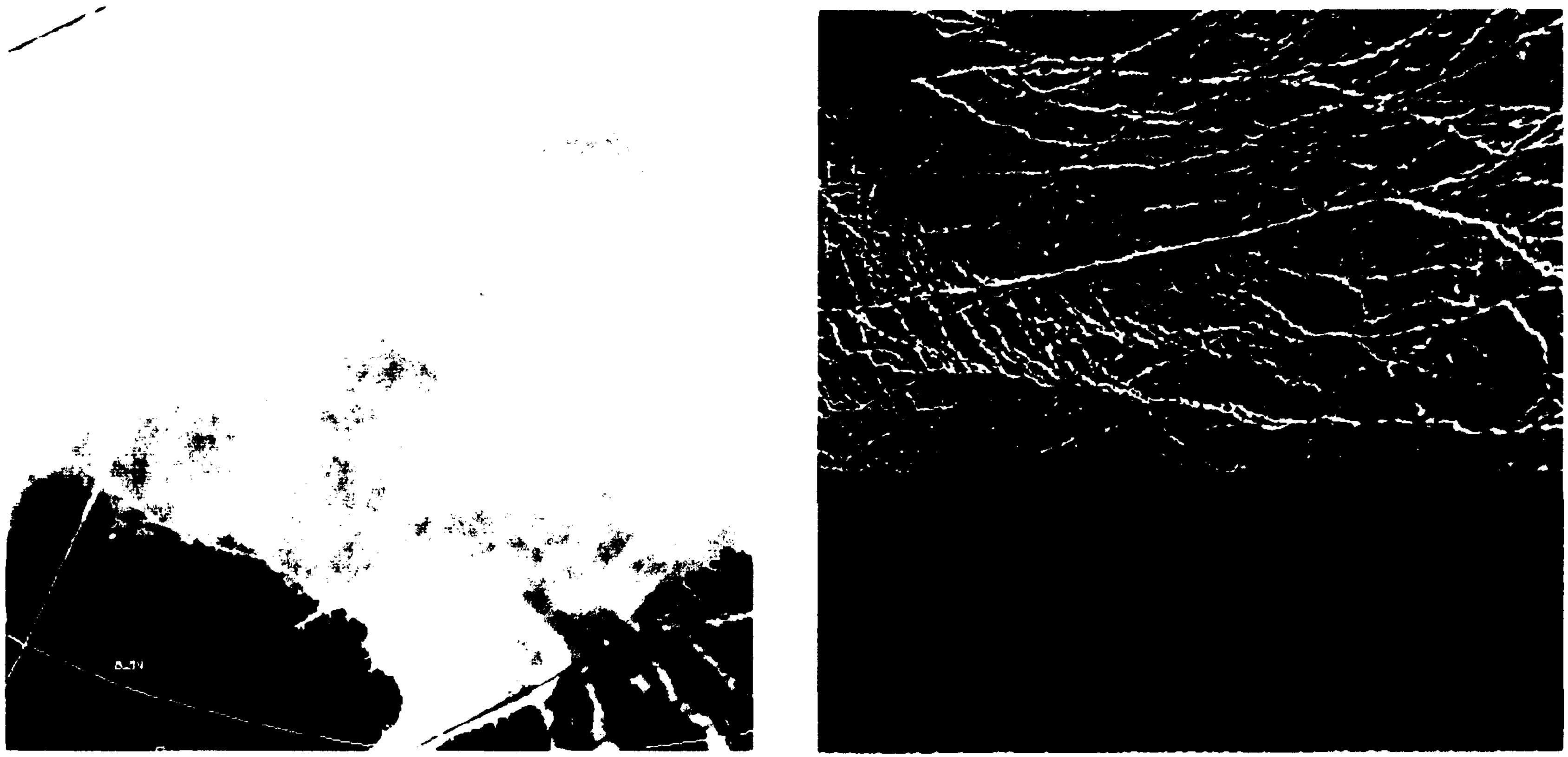

(a) (b)

Figure 4. AVHRR image from 12 January 1990: (a) infrared (channel 4) image, (b) binary image.

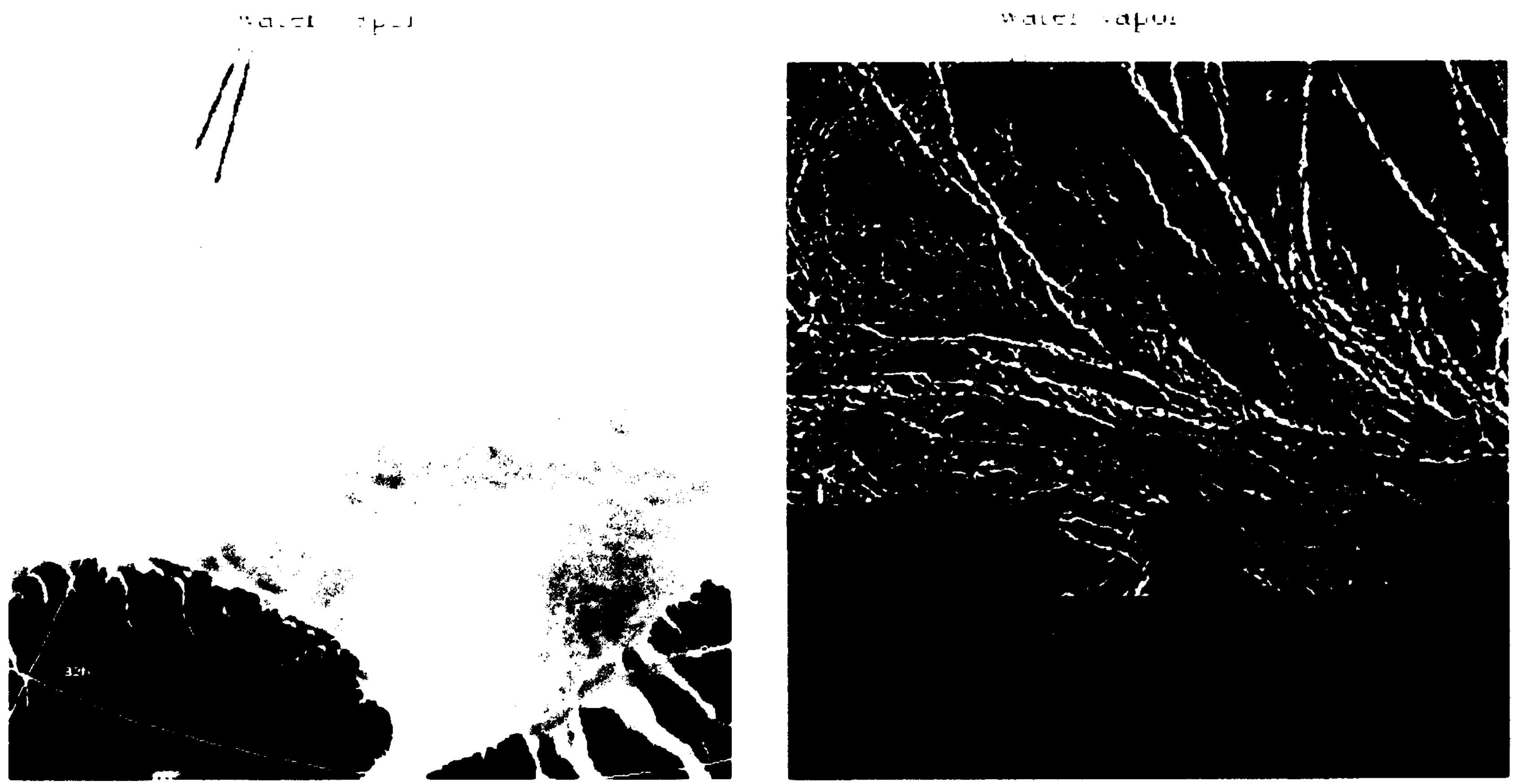

(a) (b)

Figure 5. AVHRR image from 18 March 1990: (a) infrared (channel 4) image, (b) binary image.

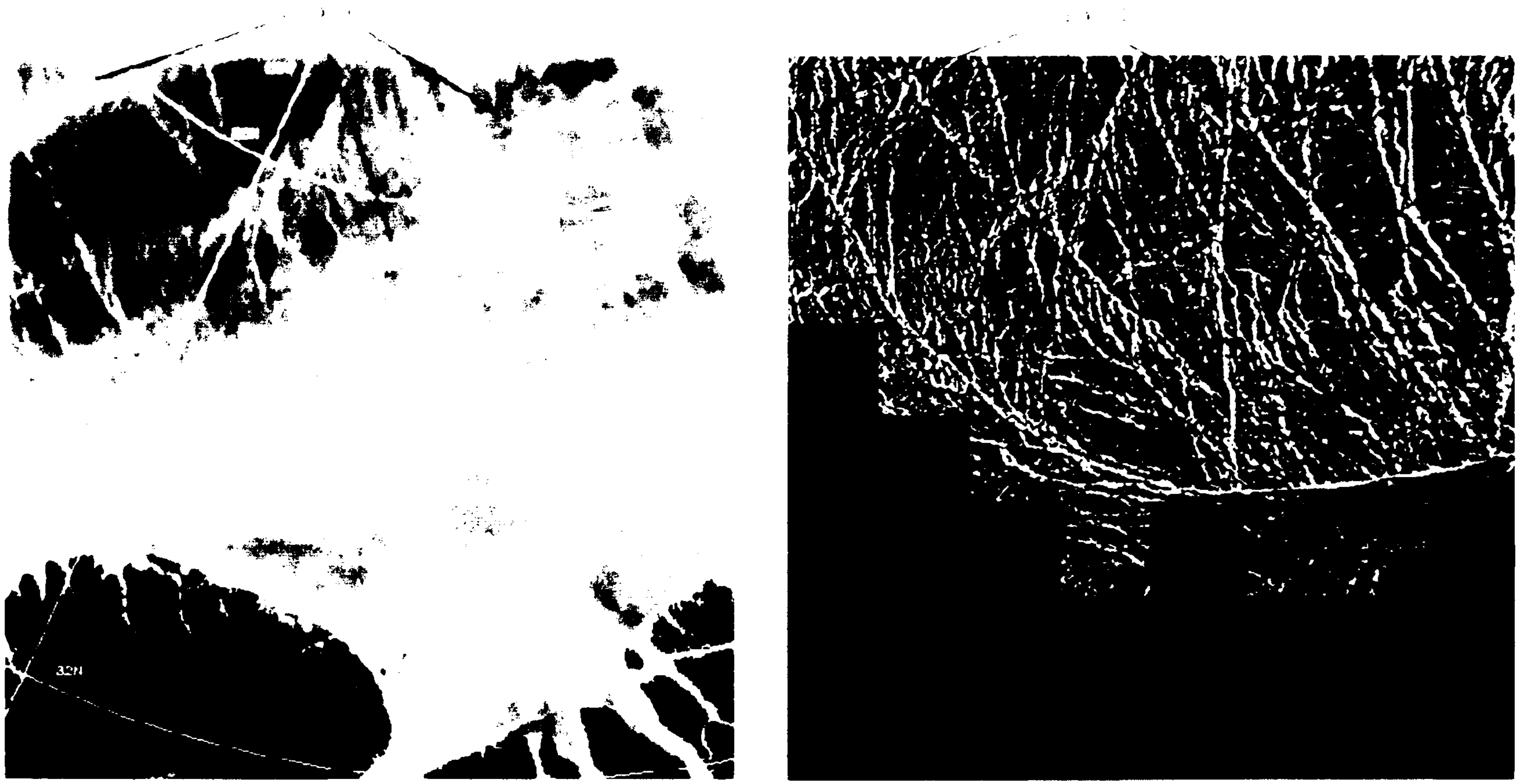

(a) (b)

Figure 6. AVHRR image from 3 April 1990: (a) infrared (channel 4) image, (b) binary image.

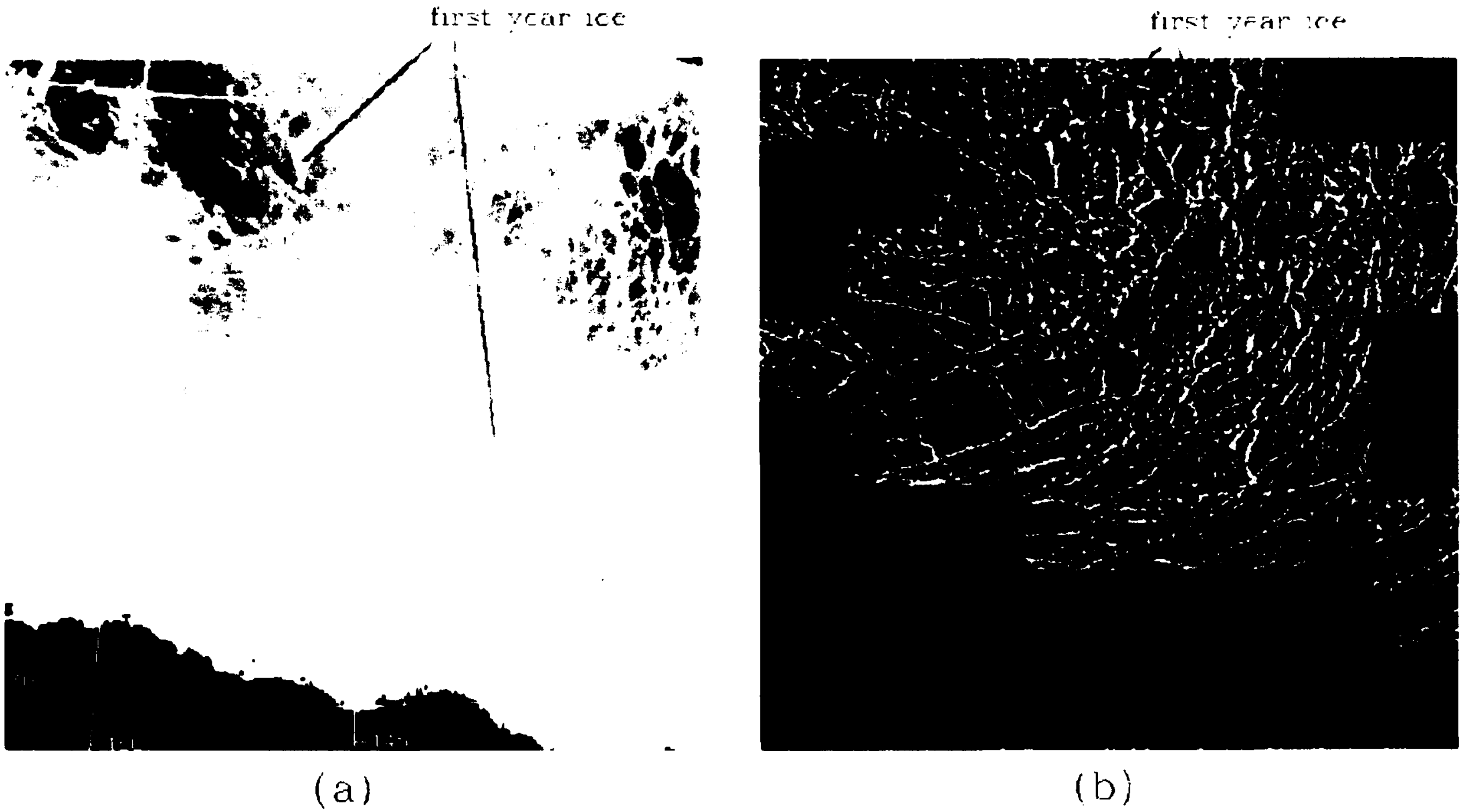

Figure 7. AVHRR image from 29 March 1992: (a) infrared (channel 4) image, (b) binary image.

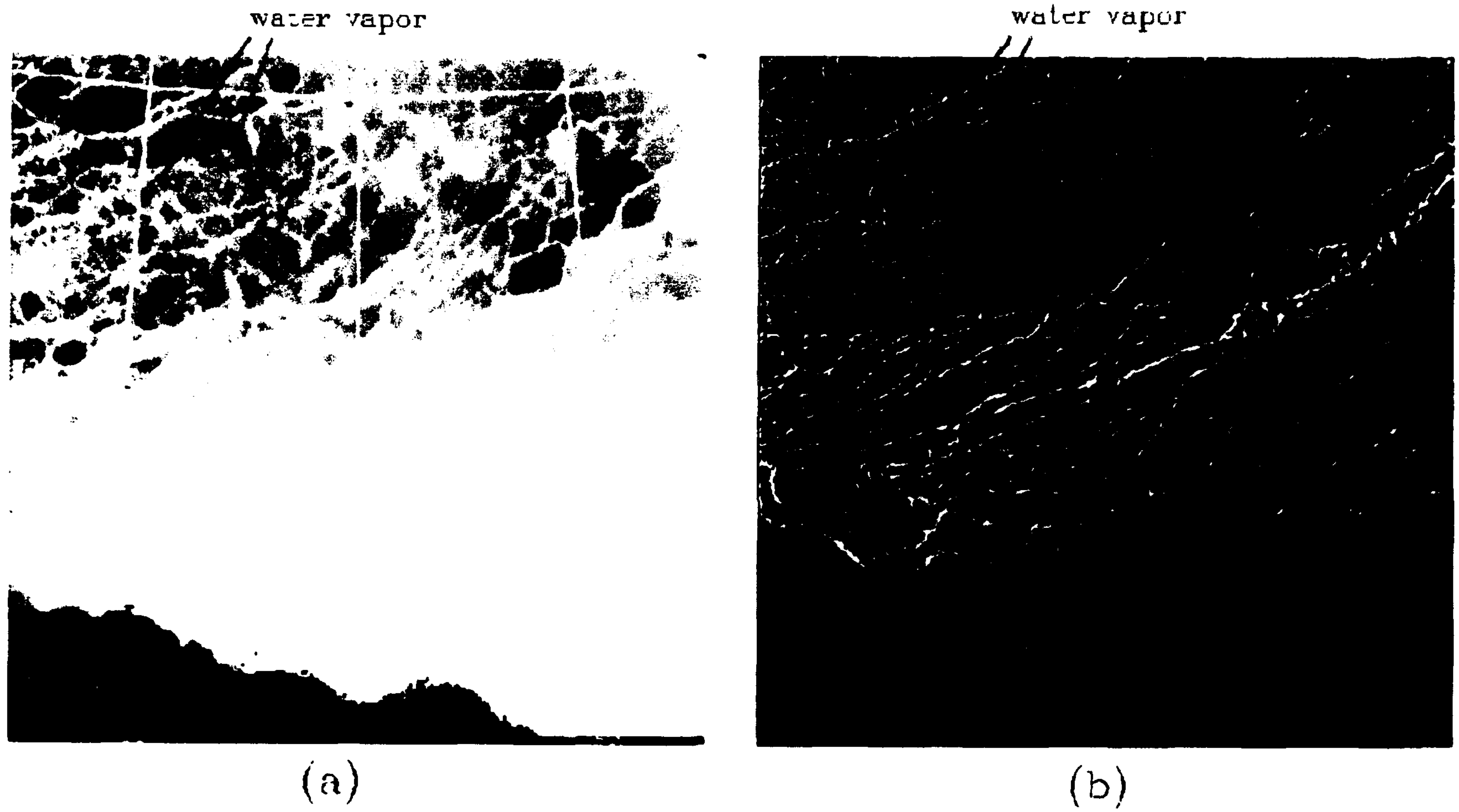

Figure 8. AVHRR image from 7 April 1992: (a) infrared (channel 4) image, (b) binary image.

specific information on which types of ice lead situations caused problems for the Hough transform technique.

The methods used to obtain lead segment results from manual lead analysis are as follows. Every 512x512 pixel image analyzed was broken up into 64x64 pixel blocks which matched those used by the Hough transform technique. For every 64x64 pixel block analyzed, a human interpreter created a trace of the leads present in the block as in Figure 9a. A software tool facilitated analysis. The size of each lead segment was calculated by totaling the number of pixels connected to a pixel which lay on the segment line within an area determined by the intersection of two circular arcs, each centered on the endpoints of the segment (Figure 9b). Lead segment orientation is calculated as the angle of the segment from vertical. The size of the lead is given by the sum of the sizes of each segment, and the orientation of the lead is given by the vector sum of the segments. Since the Hough transform technique finds relatively straight lines and does not distinguish between "lead" and "lead segment", it does not produce results for leads. The lead measurements calculated from the manual analysis are therefore not employed in this evaluation.

The manual lead analysis results are taken as truth, that is, as the best possible analysis of lead size and orientation which can be made with AVHRR infrared data. A discussion of the limitations of AVHRR data for lead analysis is beyond the scope of this report. Many small leads will not be resolved in AVHRR and measurements of lead width are only gross estimates. Key et al. (1993) provide a discussion of the detectability of leads in AVHRR data. The assumption that the manual analysis is truth is not entirely correct, since any method of analysis contains some error, but for the case of lead analysis, the human eye remains the most accurate inspection device available. Variations in the manual estimates of lead parameters due to subjectivity were minimized by having one interpreter perform the analyses over as short a time period as possible. Some error may be introduced in the lead and segment size statistics by the computer methods used to calculate lead segment size once a segment is manually defined. These errors may result in an over-estimation of the lead and segment size by the manual analysis, but the effect should be minimal.

5.0 Results

Plots which compare Hough transform analysis lead segment parameters to those of manual lead analysis for 211 64x64 pixel blocks are presented in Figures 10 through 13. Table 2 provides the tabulated statistics for the plots. For all lead segment parameters examined, the results of the Hough transform technique are correlated to the results of manual lead analysis. This correlation is especially apparent in the plots of mean segment orientation and total segment size (Figures 10 and 11). Both of these plots have relatively high correlation values (> 0.85) and slopes at or approaching one.

Table 2. Regression analysis results.

Parameter	Slope	Intercept	Correlation	RMS error	Mean Diff	Stddev diff
Total Size (sq km)	1.03	30.72	0.87	89.91	-38.95	89.58
Total # Segments	0.57	3.90	0.59	4.87	2.46	5.53
Weighted Mean Orientation (degrees)	0.74	24.30	0.88	12.82	0.68	15.22
Mean Size (sq km)	0.73	13.19	0.72	9.10	-7.46	9.69

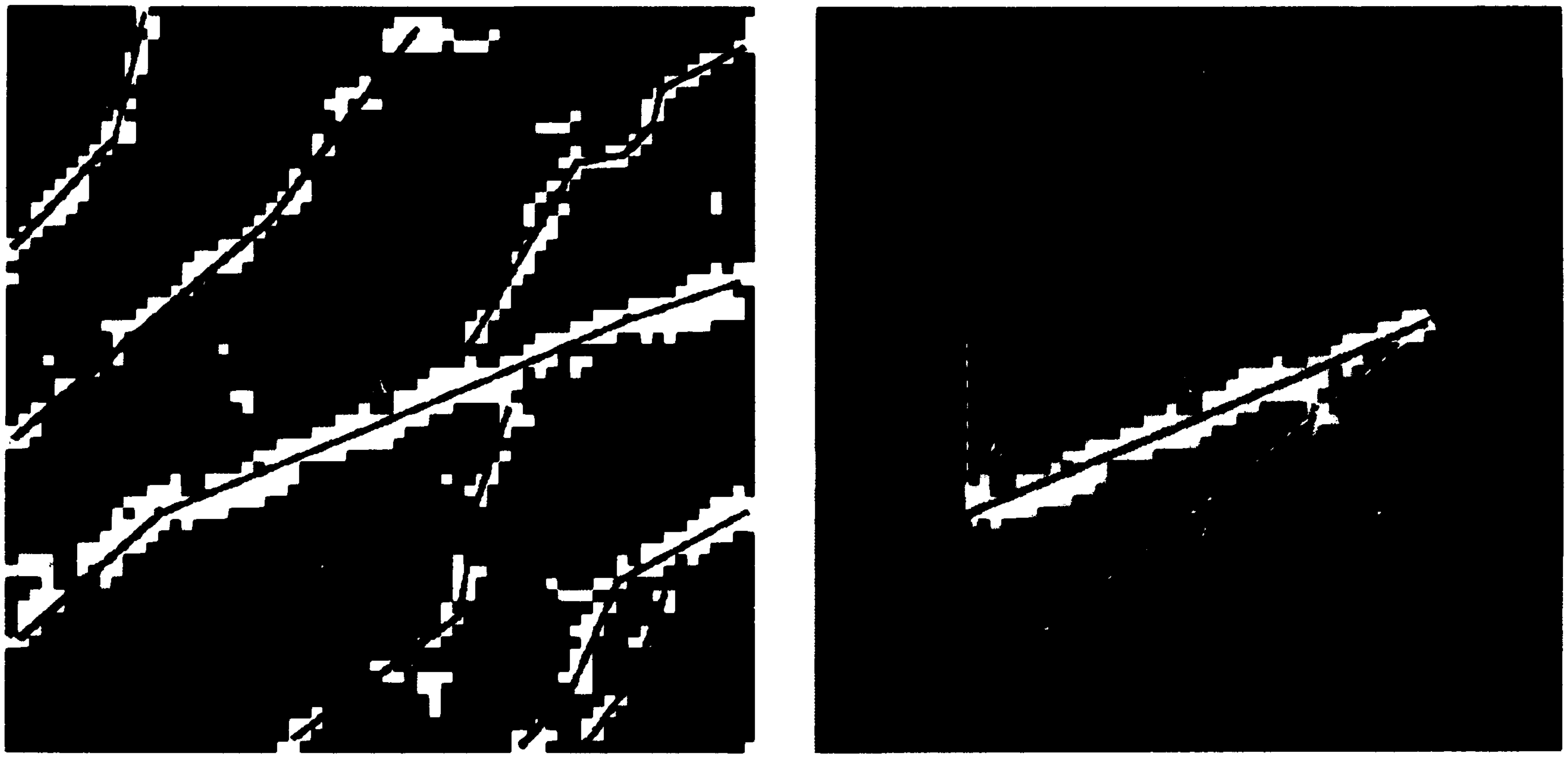

(a) (b)

Figure 9. Illustration of the manual lead analysis technique. (a) Segments are identified interactively with the red lines. (b) For a given segment A, the segment size is equal to the area in yellow and the orientation is equal to the angle from vertical to the red line.

The values of mean segment orientation appear to be the best correlated. The mean difference indicates a slight positive bias, with the manual analysis finding orientations to be on average 0.6 degrees more than those found by the Hough transform technique. The RMS error on the measurement of orientation is 12.8 degrees. Upon inspection of the plot of weighted mean segment orientation (Figure 10) the data appear unbiased until about 100 degrees and positively biased beyond 100 degrees, with the Hough transform underestimating lead segment orientation when compared to manual analysis. Further inspection of the outliers which produce this bias indicates that the bias is caused by aliasing of the orientation measurements of leads which are nearly vertical. All of the biased cases have segments whose orientation is 175-179 degrees when measured manually, while the Hough transform measurements for these same segments are in the range of 0 to 2 degrees. When the mean orientation is calculated, the 0 degree segments erroneously decrease the mean orientation value when, in actuality, the Hough technique and manual results are very close.

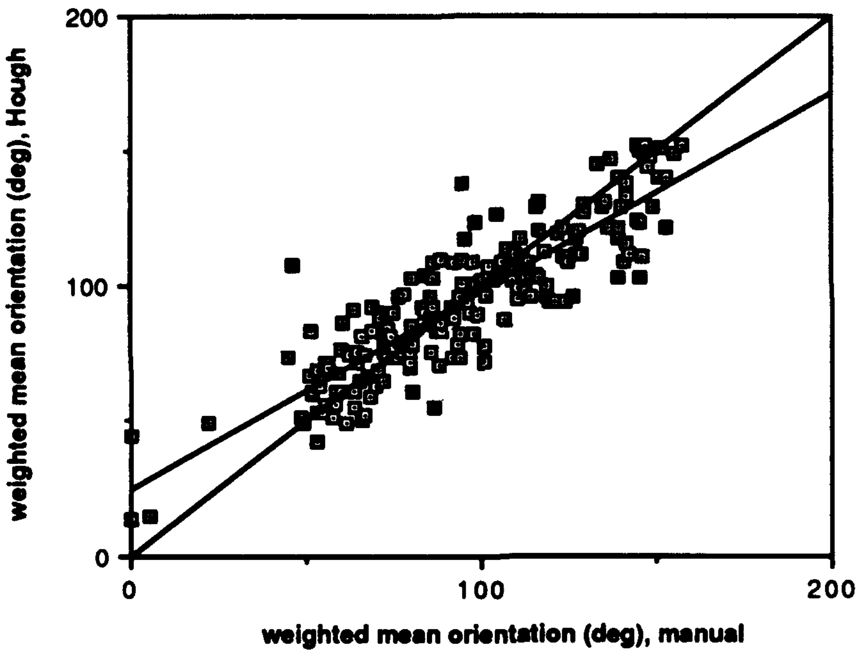

Figure 10. Manual analysis results versus Hough transform results, mean segment orientation.

The plot of total segment size (Figure 11) has an RMS error of 89.9 km^2 and a negative mean difference of 39 km^2, with the Hough transform overestimating the total lead segment size. The plot appears to be unbiased until about 150 km^2 and negatively biased beyond that. Analysis of the outliers which produce this bias indicates that the Hough transform includes some residual clouds, water vapor, first year ice patches, and other sources of noise in its measurements of lead segments. Inclusion of these non-lead features serves to falsely increase the total lead segment size calculated. These errors can be decreased through more stringent cloud masking and thresholding, and the removal of features which appear too wide to be a lead.

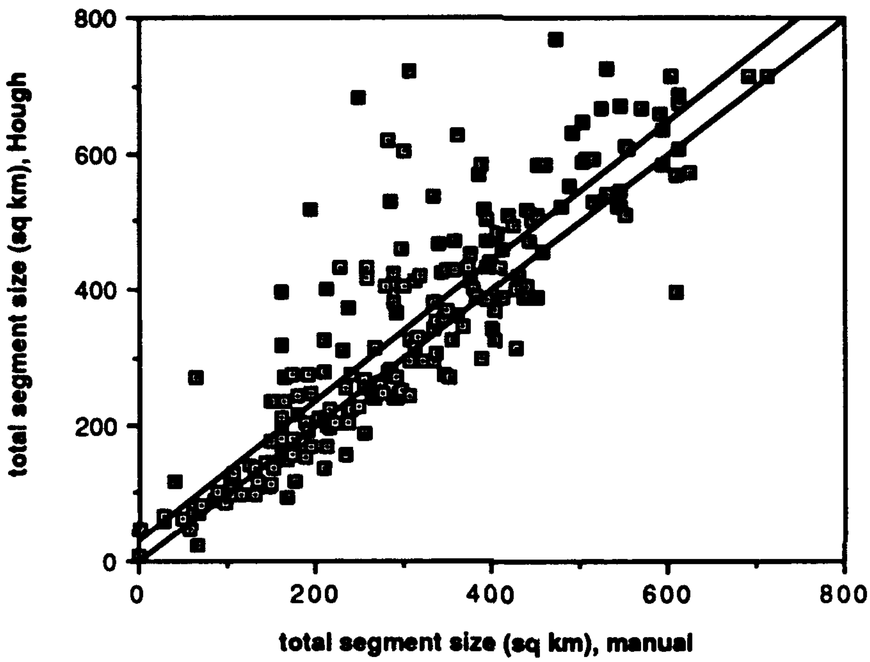

Figure 11. Manual analysis results versus Hough transform results, total segment size.

The measurements of the total number of segments, as presented in Figure 12, appear to be somewhat correlated but exhibit a positive bias and a great amount of scatter on both sides of the regression line as indicated by the large RMS error of 5 segments and the mean difference of three segments. The positive bias is to be expected. The nature of the Hough transform technique is to smear segments of very similar orientation into each other in the accumulator array. The clustering algorithm within the Hough transform technique focuses the smeared segments, but in doing so can also cluster several segments of similar, but not identical, orientation together into one (ρ,θ) point, and hence, into one segment. Upon comparison of the Hough transform and manual analysis list files it appears that the Hough algorithm clusters peaks within a range of three or four degrees. With manual analysis, segments are grouped by orientation with no smearing whatsoever, so that segments with similar orientations remain separate segments. This would cause the number of segments estimated by the Hough transform technique to be less than that estimated by manual analysis. In addition, more segments may be detected by manual analysis due to the high level of correlation which can be achieved by the human eye, and this would also cause a positive bias in the data. Misidentification of clouds, water vapor, and first year ice on the part of the Hough transform serve to create outliers on the negative side of the regression line by creating artificially high segment counts.

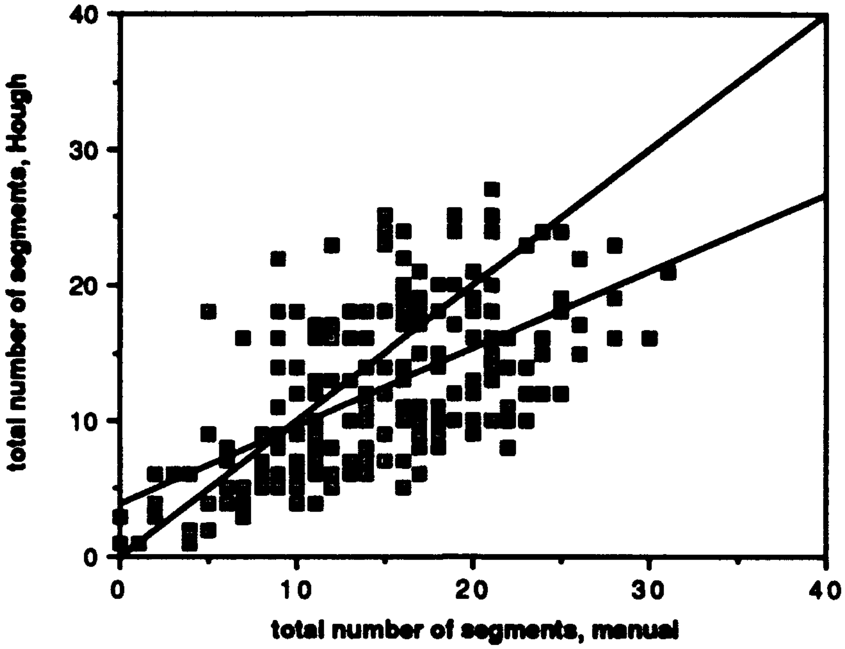

Figure 12. Manual analysis results versus Hough transform results, total number of segments.

The last plot (Figure 13) presents a comparison of mean segment size as estimated by the two techniques. The RMS error of the regression is 9.1 km^2 with a correlation of 0.72. The data are tightly clustered except for a few outliers beyond the mean size of 45 km^2. There is a negative bias to the data, but since the measurements of total segment size are well correlated and have a one-to-one relationship, the bias is probably introduced into the data by the discrepancy in the estimates of the total number of segments; the Hough transform technique consistently underestimates the number of segments, which would cause a consistent overestimation of mean segment size. Outliers on the negative side of the regression , where the Hough mean segment size are much greater than the manual mean segment size, are due to large discrepancies in the number of segments found by the different techniques. In all these outlier cases, the manual number of segments is two to three times greater than that of the Hough transform technique due to the clustering mentioned previously. Outliers on the positive side of the regression, where the Hough mean segment size is much less than the manual mean segment size, are correlated to cases where the Hough transform overestimates the number of segments because of residual cloud contamination. Disregarding these outliers, the estimates from the two techniques are well correlated.

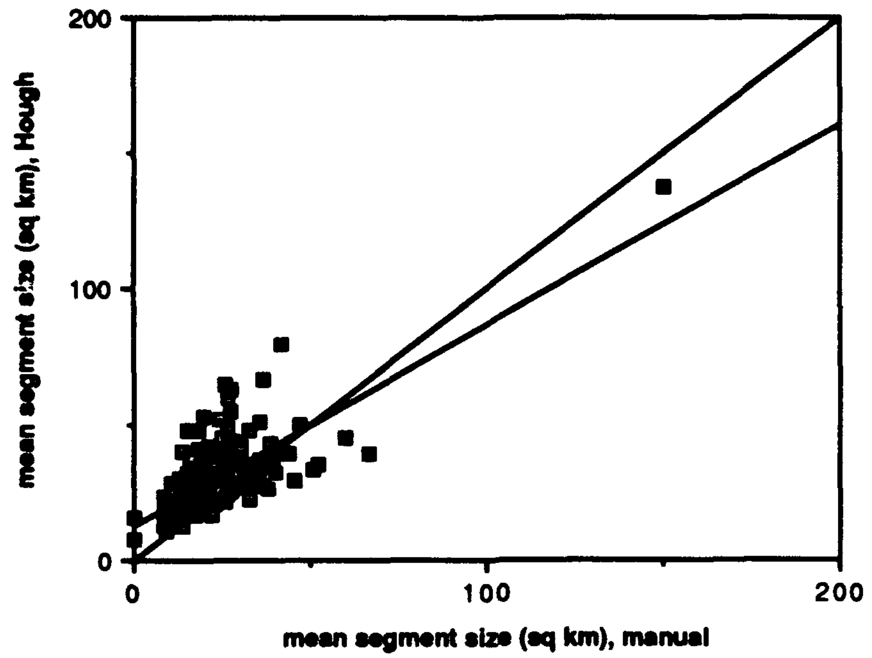

Figure 13. Manual analysis results versus Hough transform results, mean segment size.

The differences in the manual analysis and Hough transform results for each of the four parameters were plotted against orientation, total size, total number of segments, and mean size, and were found to be random, except for the bias discussed previously. There are no trends in the Hough transform results due to orientation, number, or size of the segments which are not generally seen in the manual results as well.

The histogram results (Figures 14 through 18) provide an image-by-image examination of the performance of the Hough transform. Using this analysis, limitations upon the accuracy of the technique due to variations in lead fields and the presence of other image features can be estimated. Table 3 presents a comparison of the peak locations calculated from the histograms for the Hough transform and manual techniques for segment orientation and segment size. For all cases, the distributions from Hough transform and manual analysis are well matched.

Table 3a. Histogram peak position, orientation (degrees).

Date	Location of Peaks, Hough	Location of Peaks, Manual
12 January 1990	48,95,140	48,97,145
18 March 1990	55,95,140	55,95,145
3 April 1990	7,45,100,135,175	5,90,150,170
29 March 1992	5,70,135	30,75,135,175
7 April 1992	5,48,65,140	65,175

Table 3b . Histogram peak position, size (sq km).

Date	Location of Peaks, Hough	Location of Peaks, Manual
12 January 1990	10-15	10
18 March 1990	10	10
3 April 1990	10	10-15
29 March 1992	10	5
7 April 1992	10	5

The Hough transform technique is very capable of detecting favored lead orientations present in the imagery, and provides a relatively accurate distribution of segment orientation. Figures 14c through 18c present plots of the normalized difference between between the orientation distributions for the Hough transform results and the manual analysis results. The normalized difference is calculated as the ratio of the difference in the manual and Hough results and the manual result. These normalized differences serve to highlight discrepancies in the detection of segments at given orientations. In general, the plots show differences at or fluctuating about zero, as would be expected when the Hough transform technique is performing accurately. Occasionally, misidentified features create false favored lead orientations, as is the case with the data from 18 March 1990 and 3 April 1990, where the presence of water vapor and clouds causes false peaks in the distributions at 45 to 75 degrees. The plot for 7 April 1992 also shows an overestimation by the Hough transform at about 138 degrees. This overestimation can also be seen in the histograms in figures 18a and 18b, and is due to a combination of NW/SE trending water vapor and a large lead opening which contains a matrix of floes and leads also trending NW/SE.

Figures 14f through 18f present the plots of normalized difference between the size distributions for the Hough transform and manual analysis results. For segments less than about 50 km^2 to 75 km^2 the differences are at or fluctuating about zero, indicating that the Hough transform does not disproportionately overestimate or underestimate the number of segments of these sizes. For segment sizes above 50 km^2 to 75 km^2, the Hough transform tends to overestimate the number of segments for all images. The reason for the overestimation of the number of large segments is the same as for that of the Hough transform's underestimation of the total number of segments. The clustering algorithm in the Hough transform sharpens peaks in accumulator space at the expense of the resolution of segment orientation. Peak points which vary slightly in orientation are grouped into one peak point. For example, a gently curving lead may have three segments, each with a size of 40 km^2 and orientations of 141, 142, and 143 degrees, respectively. A manual interpretation can discern these three segments but the Hough transform may cluster these segments in accumulator space, creating one 120 km^2 segment in the process. The Hough transform perceives large segments when none really exist. This tendency would produce the negative difference seen in Figures 14f through 18f at larger segment sizes.

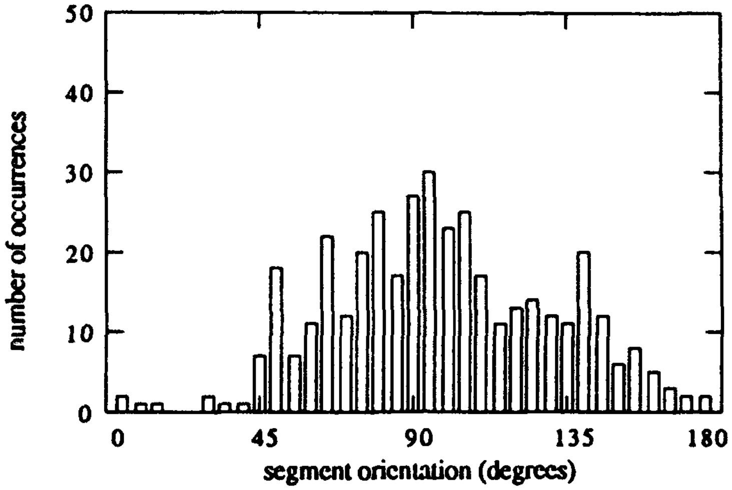

(a)

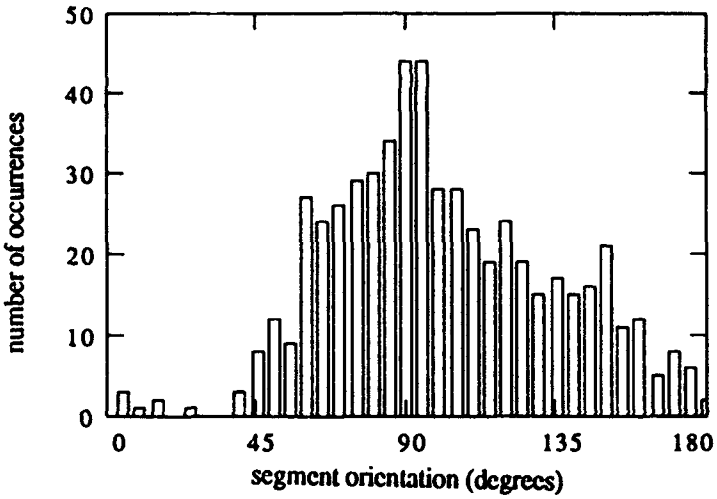

(b)

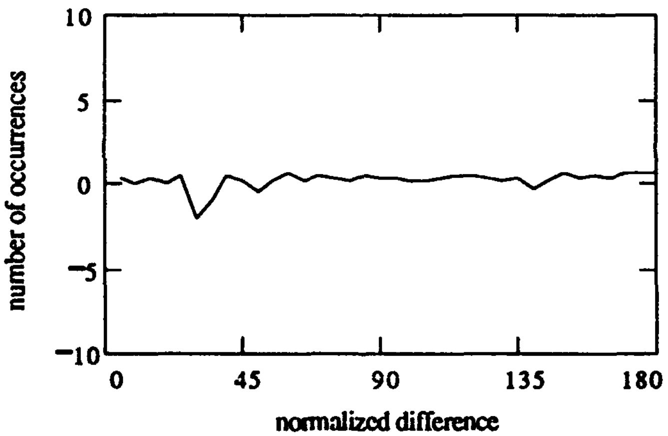

(c)

Figure 14. Histograms and difference plots for 12 January 1990: (a) histogram of segment orientation from the Hough transform results, (b) histogram of segment orientation from the manual analysis results, (c) normalized difference plot of segment orientation, (d) histogram of segment size from the Hough transform results, (e) histogram of segment size from the manual analysis results, (f) normalized difference plot of segment size.

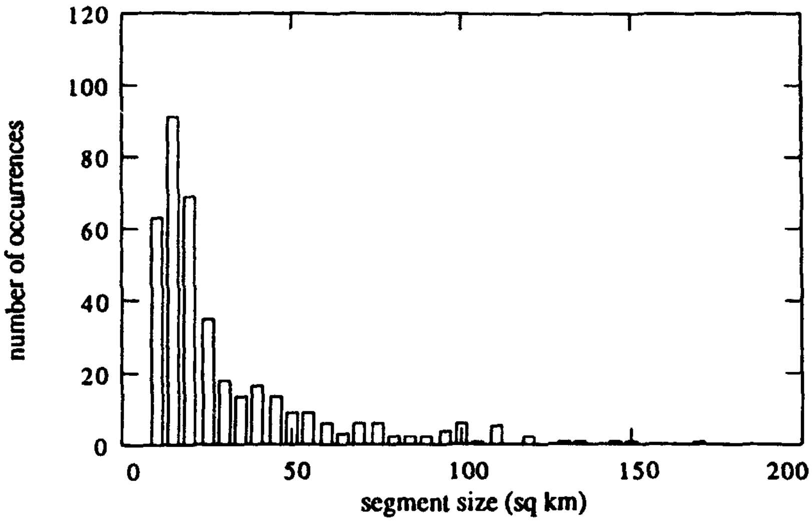

(d)

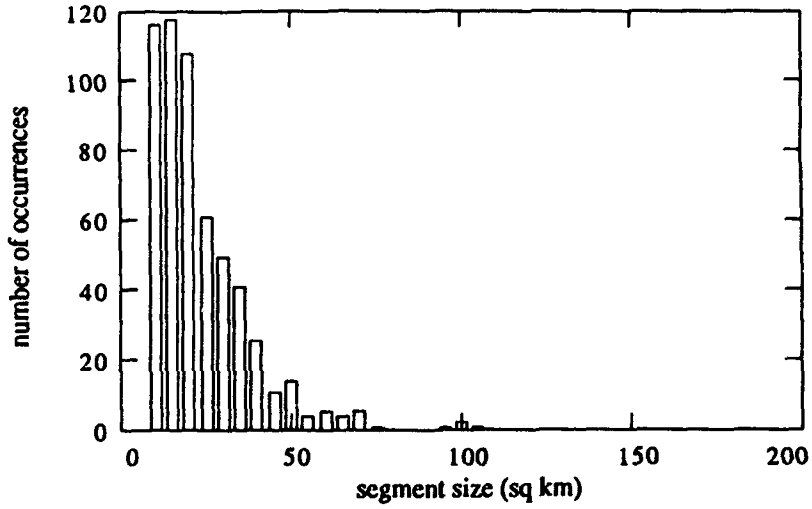

(e)

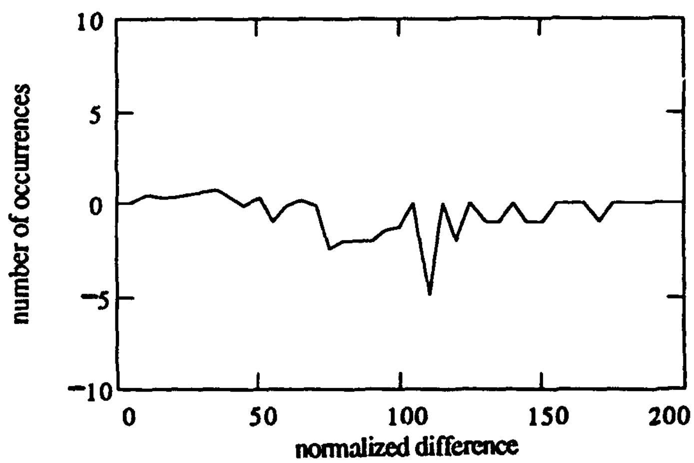

(f)

Figure 14. Continued

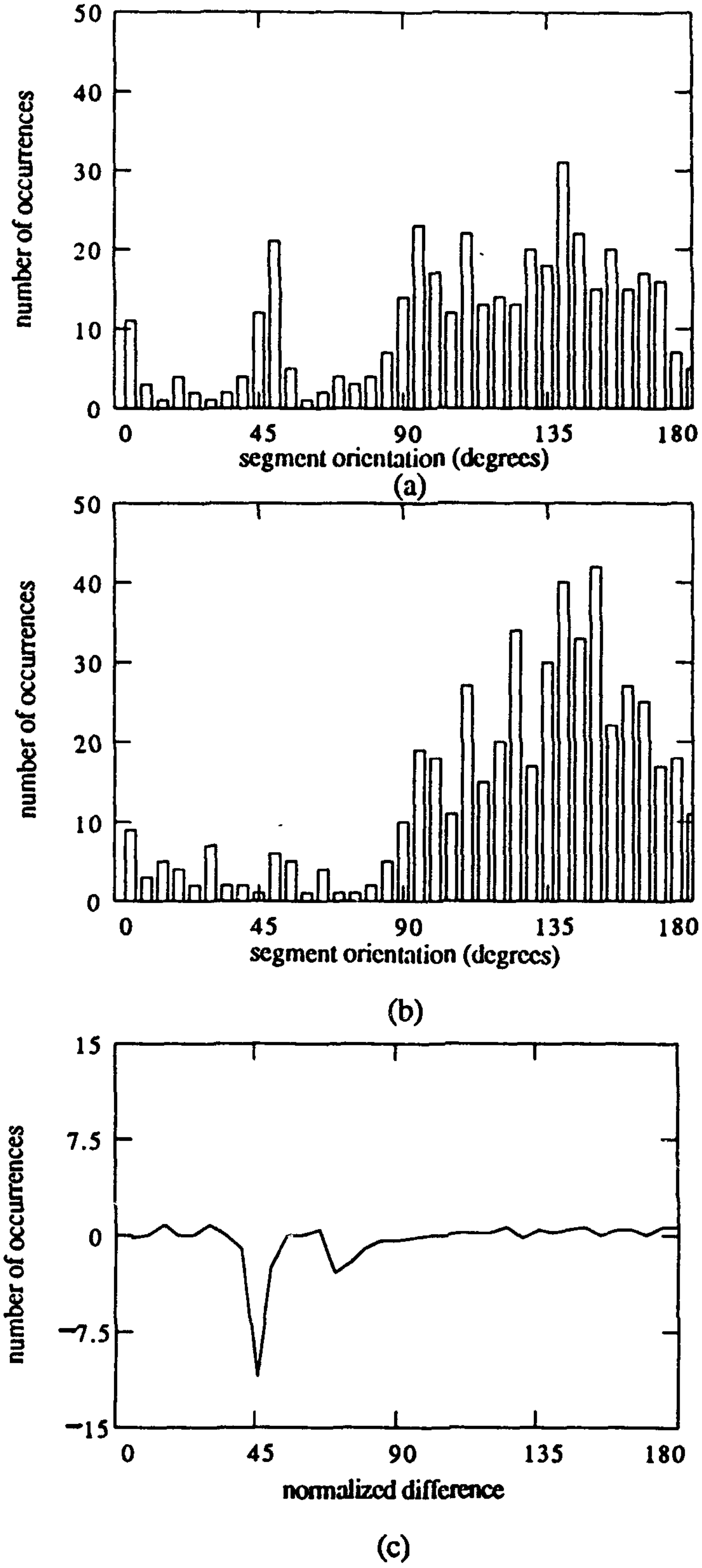

Figure 15. Histograms and difference plots for 18 March 1990: (a) histogram of segment orientation from the Hough transform results, (b) histogram of segment orientation from the manual analysis results, (c) normalized difference plot of segment orientation, (d) histogram of segment size from the Hough transform results, (e) histogram of segment size from the manual analysis results, (f) normalized difference plot of segment size.

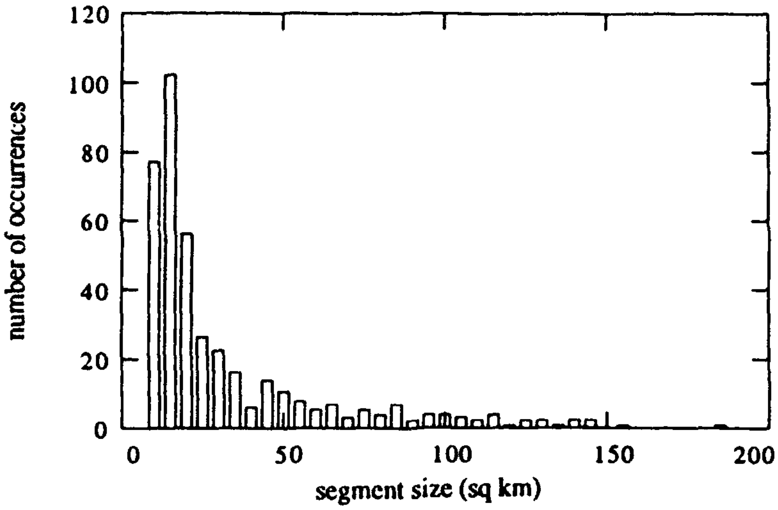

(d)

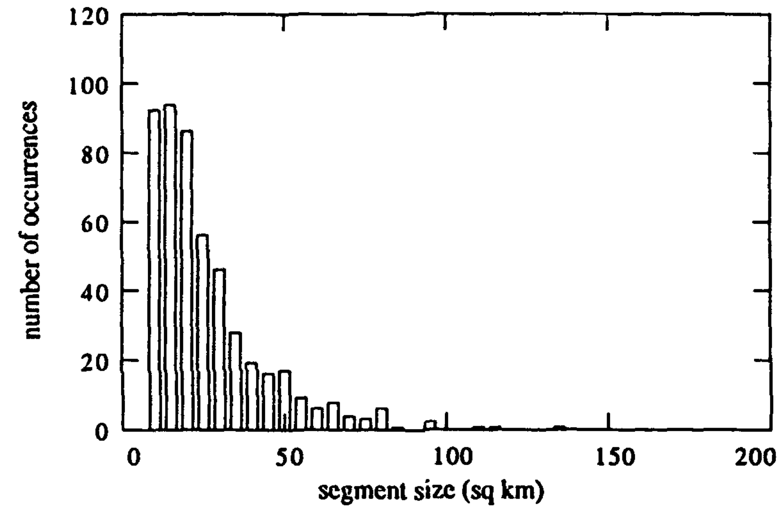

(e)

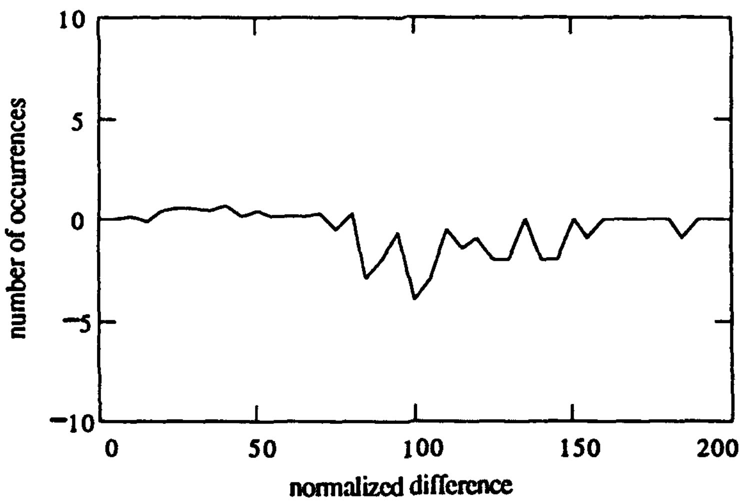

(f)

Figure 15. Continued

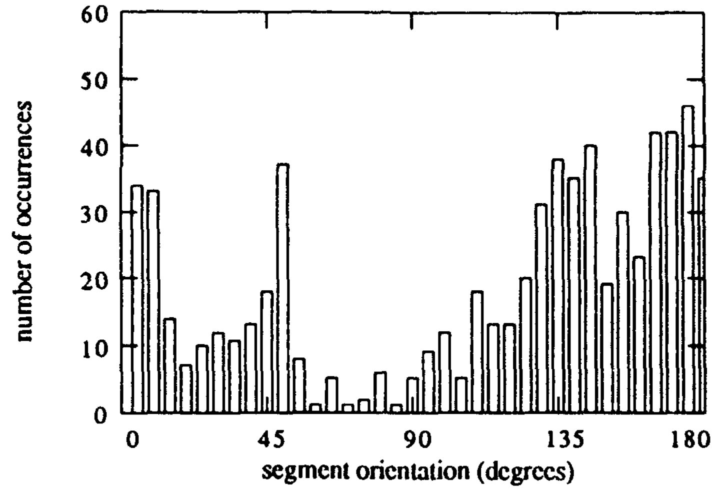

(a)

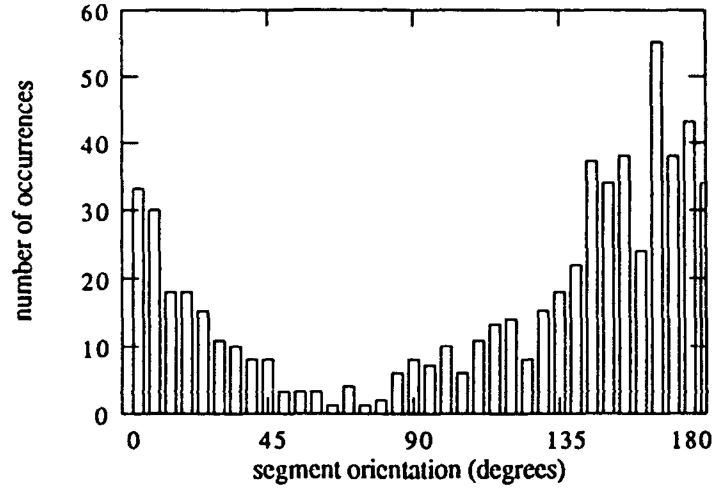

(b)

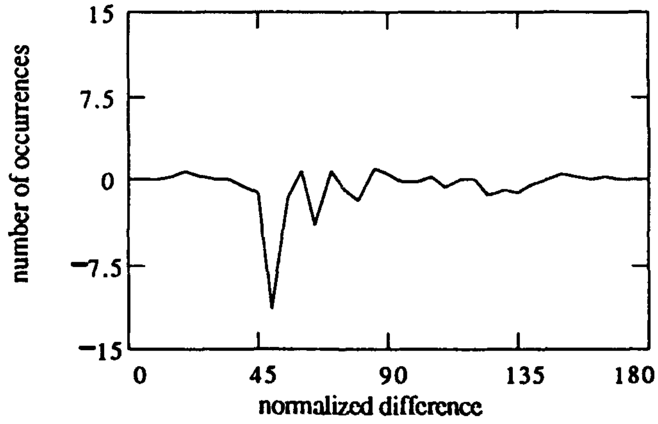

(c)

Figure 16. Histograms and difference plots for 3 April 1990: (a) histogram of segment orientation from the Hough transform results, (b) histogram of segment orientation from the manual analysis results, (c) normalized difference plot of segment orientation, (d) histogram of segment size from the Hough transform results, (e) histogram of segment size from the manual analysis results, (f) normalized difference plot of segment size.

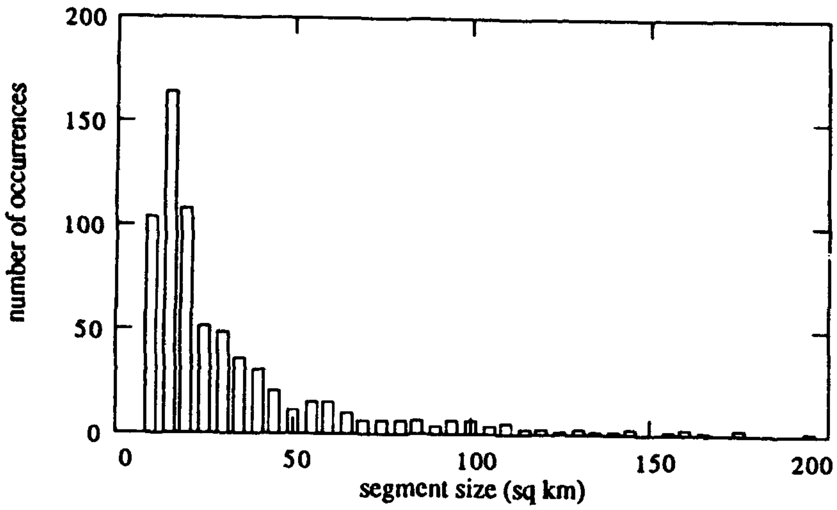

(d)

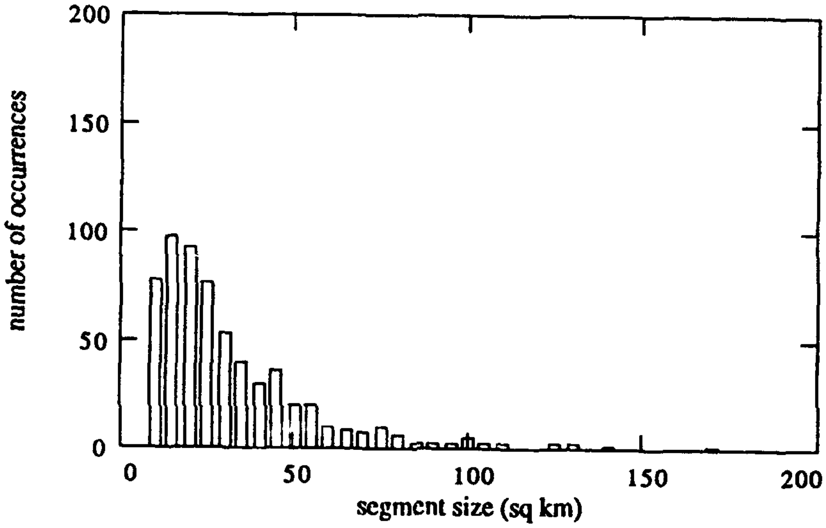

(e)

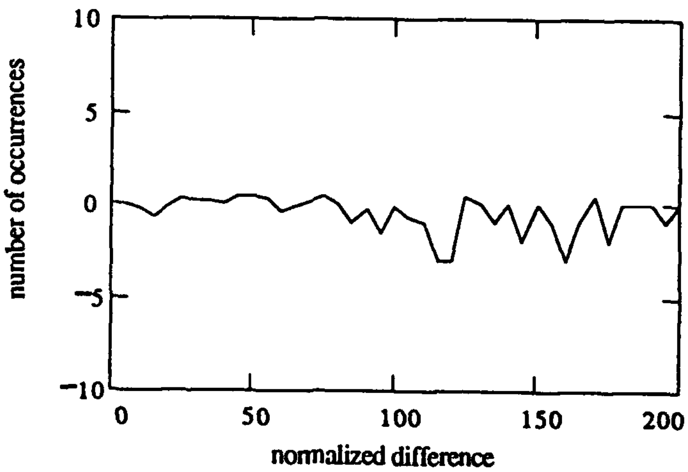

(f)

Figure 16. Continued

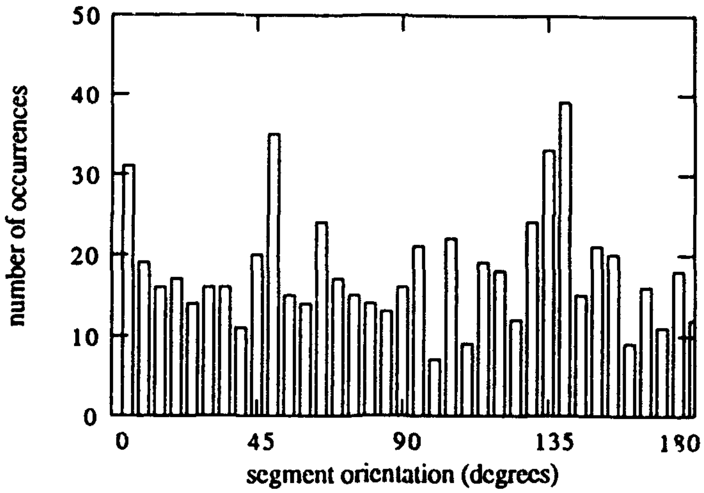

(a)

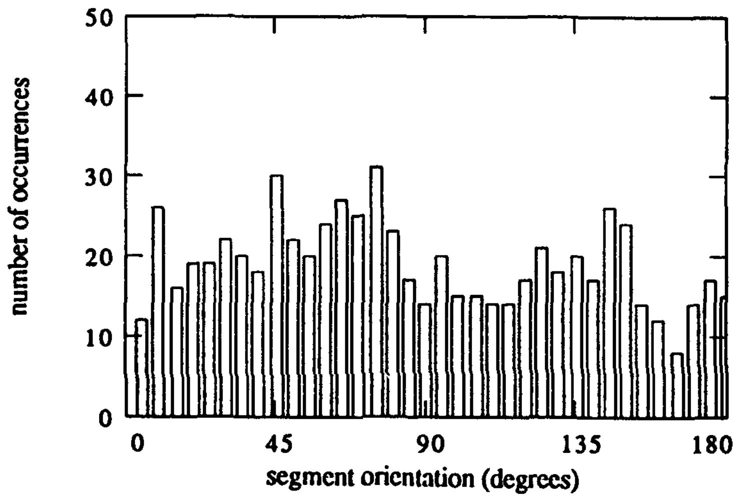

(b)

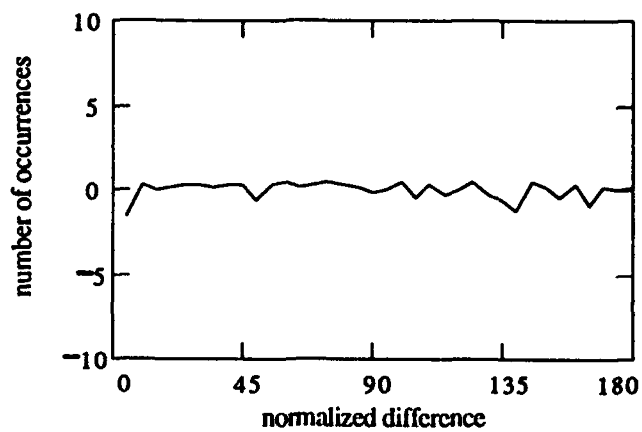

(c)

Figure 17. Histograms and difference plots for 29 March 1992: (a) histogram of segment orientation from the Hough transform results, (b) histogram of segment orientation from the manual analysis results, (c) normalized difference plot of segment orientation, (d) histogram of segment size from the Hough transform results, (e) histogram of segment size from the manual analysis results, (f) normalized difference plot of segment size.

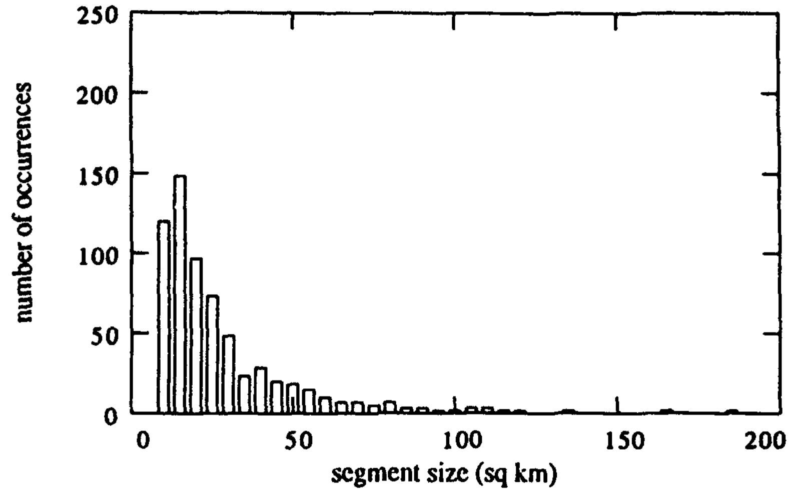

(d)

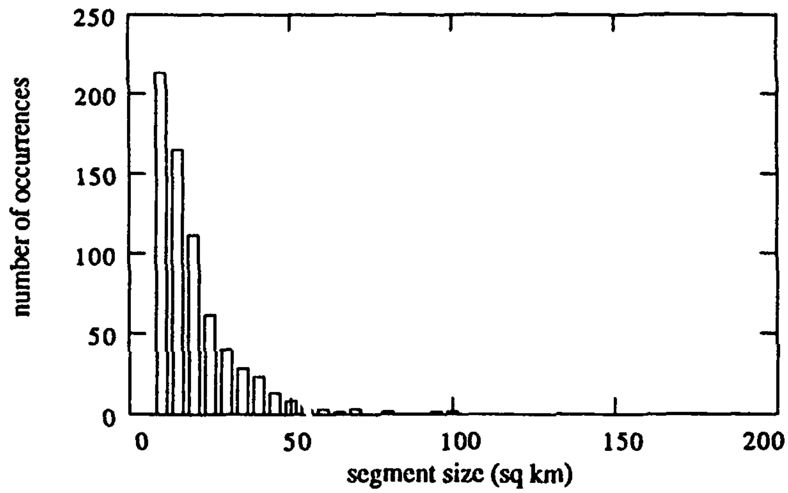

(e)

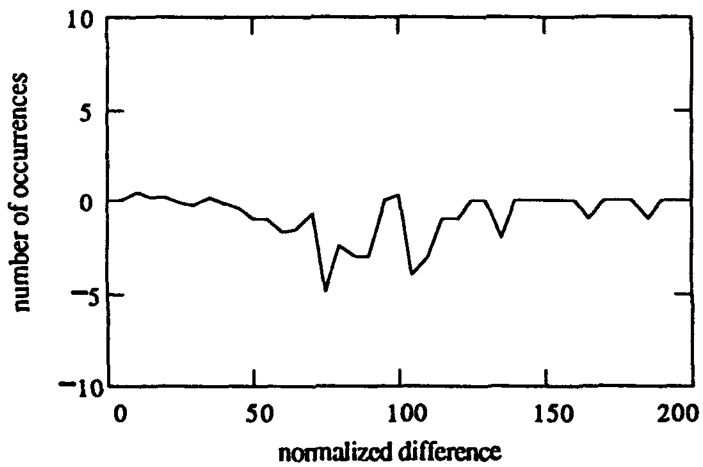

(f)

Figure 17. Continued

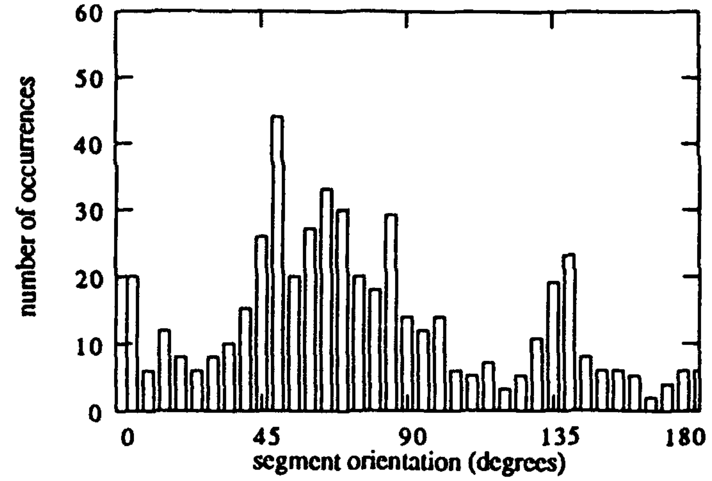

(a)

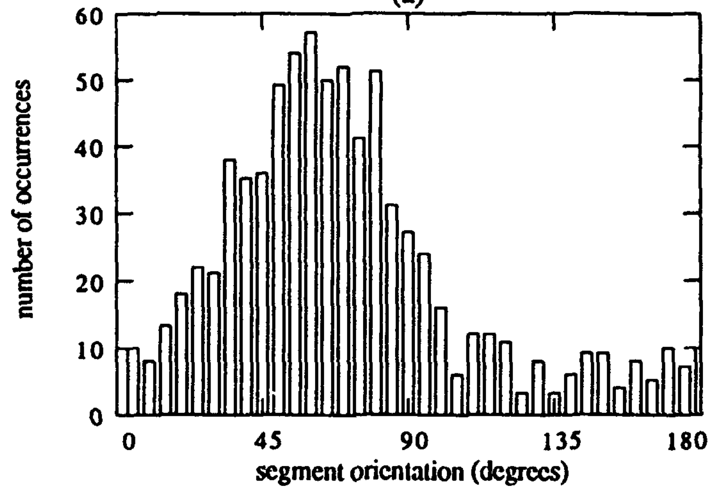

(b)

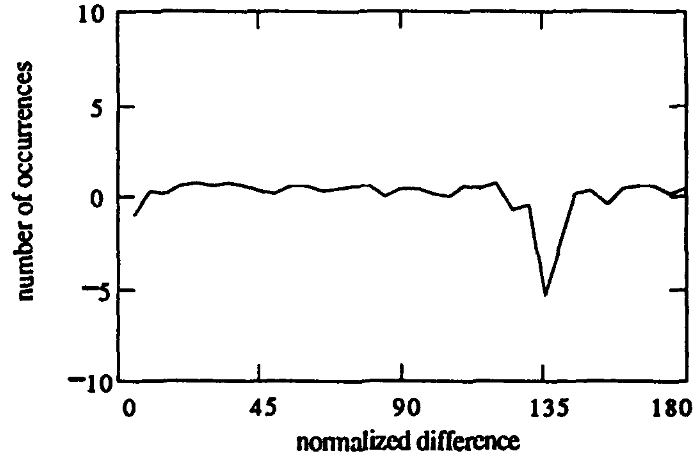

(c)

Figure 18. Histograms and difference plots for 7 April 1992: (a) histogram of segment orientation from the Hough transform results, (b) histogram of segment orientation from the manual analysis results, (c) normalized difference plot of segment orientation, (d) histogram of segment size from the Hough transform results, (e) histogram of segment size from the manual analysis results, (f) normalized difference plot of segment size.

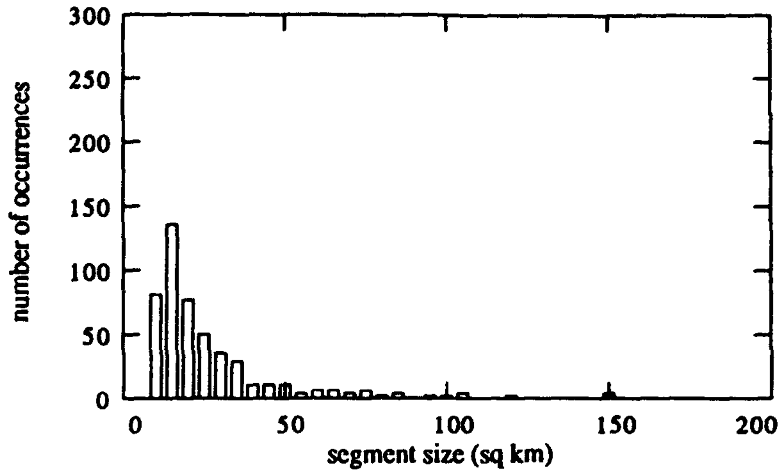

(d)

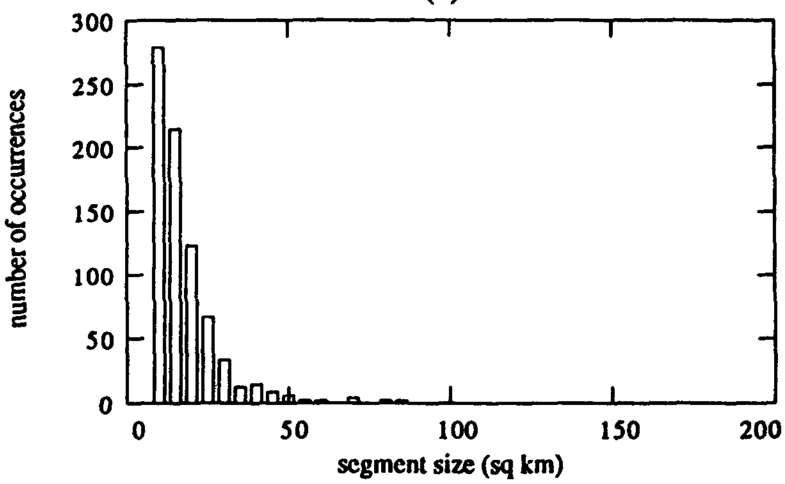

(e)

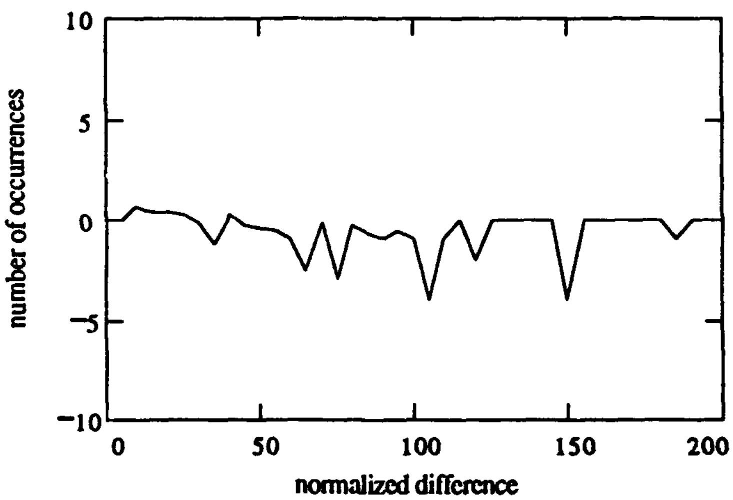

(f)

Figure 18. Continued

6.0 Conclusions and Recommendations

The Hough transform technique for lead detection has been installed into NRL and JIC processing software to aid in the automatic detection of lead features in AVHRR and OLS imagery. Use of this relatively new technique for operational means has been sporadic but should become more frequent as confidence in the technique grows. The evaluation of the Hough transform technique provided in this report serves as a first step towards the necessary increased confidence. Through the analysis performed in this report it can be concluded that:

- the Hough transform technique accurately detects the orientation of lead segments and can accurately represent the distribution of lead segment orientations within a lead field. Occasionally, false favored orientations are detected when linear features from other sources such as water vapor are present in the imagery.
- total segment size can be estimated accurately by the technique. Some over-estimation can occur in imagery containing linear non-lead features but stringent masking of the imagery can prevent this. In addition, some over-estimation of segment size may be caused by the clustering of peaks in accumulator space when lead segments have very similar (within three or four degrees) orientations. The Hough transform is capable of providing an accurate distribution of the segment sizes.
- the Hough transform under-estimates the number of lead segments in an image. This error is due to clustering of segments in accumulator space and could be decreased by fine tuning cluster parameters.
- mean segment size determined by the Hough transform, since it is dependent on the estimation of the number of lead segments, is also inaccurate.

In general, the Hough transform can and should be used with confidence for the estimation of lead segment orientation and total lead segment size from AVHRR imagery which has been well masked.

Recommendations for improvements in the accuracy of the technique are to:

- stringently mask and filter imagery to remove as much cloud and water vapor contamination as possible. Removal of these non-lead features prior to the application of the Hough transform technique will improve the segment size and segment number estimates.
- set up a threshold in the algorithm for segment width. Such a threshold would provide a filter by which the algorithm could remove the effects of non-lead features which are bright, but very wide, such as patches of clouds or first year ice floes.
- automate the pre-processing procedures. This would make the Hough transform technique operationally more efficient and easier to use. The Wallis filter could be easily automated in the algorithm. The interactive binary thresholding would be more difficult to automate but could be implemented once an average threshold value has been established for the imagery.
- fine tune the internal parameters of the noise thresholding in accumulator space and of the clustering algorithm. Noise threshold and clustering parameters of the algorithm should be varied depending upon the type of lead field analyzed. This would make the algorithm run more accurately.
- add a function which would enable the transform to determine the ends and intersections of leads. Segment statistics can provide information about lead statistics if the leads and segments are proportional; that is, if there are no wild fluctuations in segment orientations or size in the lead field. True lead statistics, rather than segment statistics, however, are generally more desirable to the user community.

7.0 References

Fetterer F. and R. Holyer (1989). A Hough transform technique for extracting leads from sea ice imagery, Proceedings, International Geoscience and Remote Sensing Symposium, Vancouver, British Columbia, July 10-14, pp. 1125-1128.

Fetterer F., A. Pressman, and R. Crout (1990). Sea Ice Lead Statistics From Satellite Imagery of the Lincoln Sea During ICESHELF Acoustic Exercise, Spring 1990, Naval Research Laboratory, SSC, MS, NOARL Technical Note 50.

Key J., J. Maslanik, and E. Ellefsen (1993). The effects of sensor field-of-view on the geometrical characteristics of sea ice leads and implications for large-area heat flux estimates, submitted to Remote Sensing of Environment, September 1992.